

2D Friction Anisotropy of Micro-Pillared Surfaces for the Translation of Small Objects

Will Langford, Jifei Ou, Lining Yao
MIT 2.675 - Micro/Nano Engineering Laboratory
December 5, 2014

Abstract:

We propose a novel two-dimensional translation system for small objects. The system consists of surface of oriented micro-pillars and a vertical vibration source with tunable frequency and amplitude. Preliminary tests show that our system is able to control the movement and velocity of small parts through the arrangement of the oriented pillars and control of the vibration frequency and amplitude. We show that a simple beam bending model fails to capture the full dynamics of the pillar-object interaction and suggest a hybrid dynamic model as future work. In this study, we describe and compare two fabrication approaches we pursued as a means of producing these surfaces: stereolithography and laser micromachining in conjunction with replica molding. We further provide test results showing that both the frequency and amplitude of the vibration source are linearly related to how fast an object moves on the surface. Finally, we propose potential applications for this system which include ways to sort parts by size and weight.

I. Introduction

As microfabricated devices become increasingly complex, researchers have been looking for better ways to move and manipulate individual parts at these scales. Inspired by the cilia structure of natural organisms, our work shows how structured surfaces of oriented micro-pillars, subject only to a single global vibration source, are able to predictably transport, orient, and possibly screen small parts.

There are numerous examples of natural systems that take advantage of natural vibrations and employ anisotropic mechanical structure as a means of generating differential friction used for locomotion or particle transport. Many insects, for example, use rigid hair-like setae on their legs as a mechanism for removing debris and particles.^[1] Similarly, the ciliary arrays lining the inside of our lungs produce surface standing-waves that propel a mucus layer of contaminants over the surface.^[2]

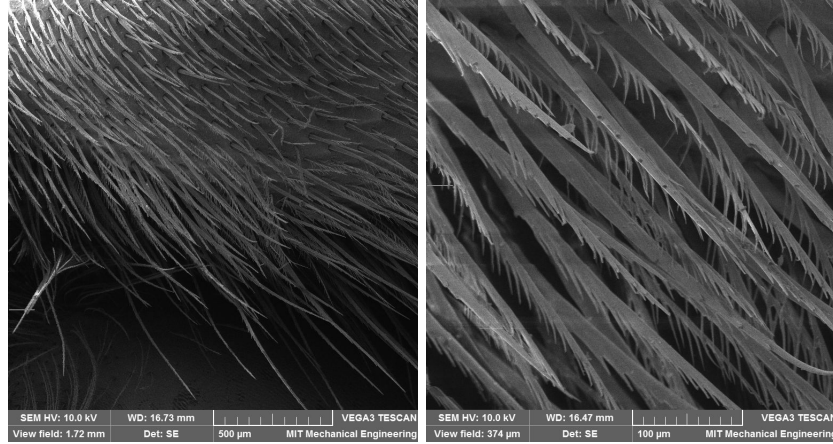


Figure 1. The setae of a honeybee is as an example of anisotropic “hairy” structure.

In man-made machines, on the other hand, small parts are traditionally conveyed using belts or vibrating surfaces. These mechanisms are either limited to simple one-dimensional translation or unable to independently control the transport of individual parts.

Previous research has looked to scale down these kinds of conveyance systems to enable the control of individual micro-components on a two-dimensional surface. These systems may use arrays of MEMS actuators,^{[3][4][5][6][7]} tilted air jets,^[8] or electromagnetic coils,^[9] among other techniques to translate, orient, and arrange parts on a surface. These techniques involve complex design (multiple moving parts per actuator), complex fabrication (typically a many-mask photolithography process), and complex control (because there are n^2 actuators).

In contrast to much of the prior work done in two-dimensional micro-conveyance systems, our approach is simple and scalable, relying only on a relatively-simply structured surface and a global vibration source. Our strategy is similar to the way in which “bristle-bots” move. A bristle-bot, which is composed of a rigid body with an array of compliant legs, moves by exciting a vibration with an onboard oscillating mass. The vibration causes the legs to stick and slip on the horizontal surface and propel the robot forward. This simple technique is surprisingly effective and has been shown to propel robots at many times their own body-length per second.^[10] Our micro-pillared surfaces effectively invert this bristle-bot mechanism and leverage it to move objects on a surface without the need for precise control of an array of actuators.

II. Modeling Pillar-Object Interactions

There are a number of techniques that have been used to model vibration induced movement with both “hairy” and conventional structures. The most relevant of this literature analyzes the way in which bristle-bots move. As described previously, a bristle-bot is typically made of a rigid body with flexible legs. The legs contact a horizontal surface at an angle and through the oscillation of an onboard mass, the robot propels itself across the surface by taking advantage of stick-slip effects.^[10] Mathematical models of bristle-bots are formulated in a few different ways but nearly all make the same general assumptions. First, the robot’s legs may be modeled by massless rigid links attached to the main body by a torsion spring of some constant stiffness.^[11] Second, the legs are always in contact with the surface, which means

the acceleration of the robot upward must never exceed gravity.^[12] Finally, the interaction of the legs with the surface is modeled by dry coulomb friction and the assumption is made that forward motion occurs because of stick-slip caused by an oscillating normal force at the leg-surface interface.^[10]

We predicted that much of the same assumptions hold for our microstructured surfaces. Our hypothesis was that forward motion of an object on the surface is achieved by the stick-slip effect caused by a repeated increase and decrease in the normal force acting at the leg-object interface. Figure 2 illustrates this stick-slip effect for a single micro-pillar during one cycle of surface oscillation.

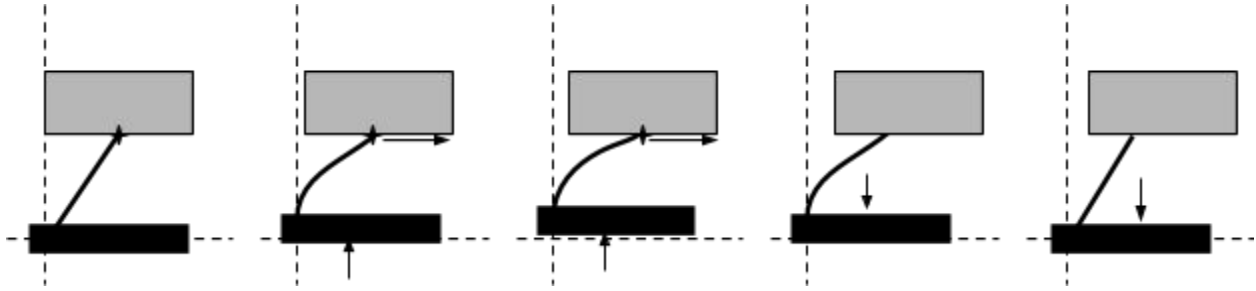


Figure 2. One cycle of the stick-slip mechanism.

Under this assumption, a first approximation for the distance an object travels during a single cycle can be calculated using the fixed-free cantilever beam bending equation. To do this, we make a number of assumptions about the geometry of both the pillars and the object (shown in Figure 3).

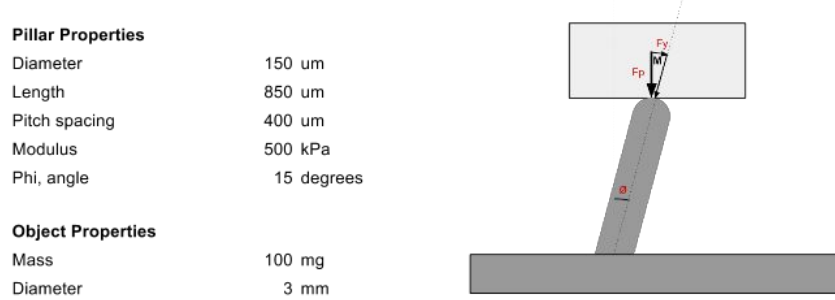


Figure 3. Pillar and object geometry used in calculations

We can first examine the amount of deflection of the pillars due to the weight of the object alone:

$$\delta = mg * p^2 / (\pi d^2) * L^3 / (3EI) * \sin(\phi) \cos(\phi)$$

$$\delta = 40 \mu\text{m}$$

If we assume that the inertia of the object is large compared to the acceleration of the surface upwards, this deflection increases. We can calculate the deflection the pillar would experience as the surface is driven with a 100Hz sine wave with a stroke of 0.1mm:

$$a_{\text{accel}} = A\omega^2$$

$$\delta = (g + a_{accel})m * p^2/(\pi d^2) * L^3/(3EI) * \sin(\phi)\cos(\phi)$$

$$\delta = 201\mu m$$

These calculations provide a crude estimate of the distance an object travels per period on the micro-pillared surface and allow us to make predictions of how the performance scales with various parameters. For example, it is clear that, under these assumptions, amplitude should be linearly related to the velocity with which an object travels on the surface. We can also predict that, for a sine wave, frequency is quadratically related to velocity since the acceleration of the platform scales with the square of the frequency. This model also predicts that heavier objects will move faster; however, intuition suggests that this is only true until the deflection of the pillars becomes significant compared to their length.

While this model helps us predict general trends and relationships between parameters, as we show in the results section, it fails to capture the real-world dynamics of this system. The 200 μm deflection predicted by this model is more than three times smaller than what the physical experiment showed.

In order to capture the full dynamics of this system, a new approach is needed. One possible modeling technique that may be used effectively here is a hybrid dynamic simulation. This kind of simulation incorporates both discrete and continuous dynamics and transitions between states.^[13] This dynamic model would consist of two states: one in which the object is in contact with the pillars and one in which the object is in the air. When the object is in contact with the pillars, the system can be thought of as an idealized mass-spring-damper system. The shape and stiffness of the pillars governs the effective spring and damping constant while the mass of the object governs the inertial term. When the object is in the air it is simply governed by the acceleration of gravity. The transition between these states occurs when the spring passes through its free length. This kind of model would be able to take into account the much more dynamic nature of the pillar-object interaction that we see in the experimental results.

III. Fabrication

In order to create an effective translating path for the objects, we need to accurately design and fabricate the micro-pillars. In this study, we explored two parallel methods of digital fabrication.

A. Stereolithography

Stereolithography promises an easy way of constructing oriented pillars. Here, we present method of bitmap printing and geometric modelling, enabled by the micron-scale feature sizes in today's 3D printers.

The stereolithography fabricated samples are printed by Autodesk Ember Digital Light Processing (DLP) 3D printer. The printer has the feature resolution of 50 μm on X and Y axis, and 10 μm on Z axis. The build volume is 64 by 40 by 150 mm. The used print material is near UV light photopolymer (Available on <http://formlabs.com>). For our test sample, we set the layer exposure time to 2.8 seconds for an optimized polymerization time.

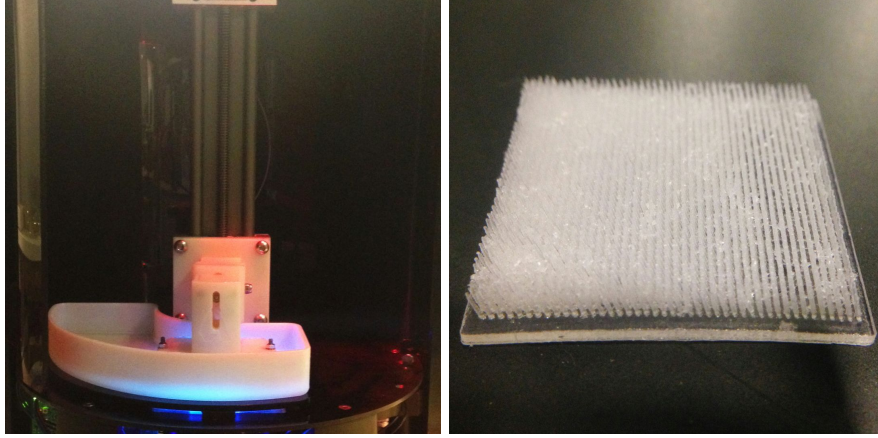


Figure 3. Printer in operation (left). 3D-printed micro-pillared surface (right).

Conventional workflow of stereolithography for a designed object starts with an geometrical mesh. In our study, as we need an array of microscale pillars, it requires high computational capacity to process such large quantity of meshes. DLP provide a pixel-by-pixel, layer-by-layer method to create 3D geometry. We decide to build a program that renders printing bitmaps to recreate 3D shape. This gives us the space to manipulate pixels, therefore give us higher controllability of the pillar geometry.

The shape of a pillar is a cone with high aspect ratio. As we know, the diameter of cone continuously decrease from the base to the tip. However, the smallest unit in DLP printer is pixel. Therefore we need to find a way to construct a model that could approximate the geometry of a cone. As shown in Figure 4, we set the base of a pillar to be 3 by 3 pixels. That gives us a diameter of 150 μm . As the layer increases, the pixels reduce in a spiral manner, leaving the top layer with just 1 pixel. This method gives us the highest resolution control of the printed cone shape. For tilting the hair to a certain angle, we can offset the pixel group every certain layers. the relationship of tilted angle and layer is:

$$\tan\theta = L * 5 / P$$

where L is the number of layers, and P is the numbers of pixel.

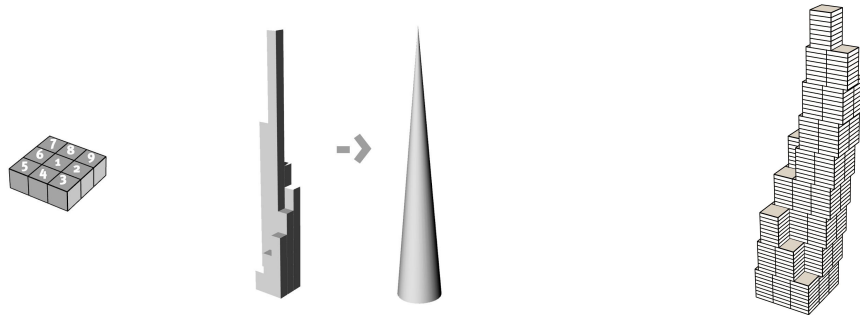


Figure 4. Simulation of Pillar Geometry Modeling. Left: straight. Right: tilted.

We successfully printed a series of sample surfaces with oriented hair. Figure 5 shows that our printed geometry matches the computer simulation (Figure 4).

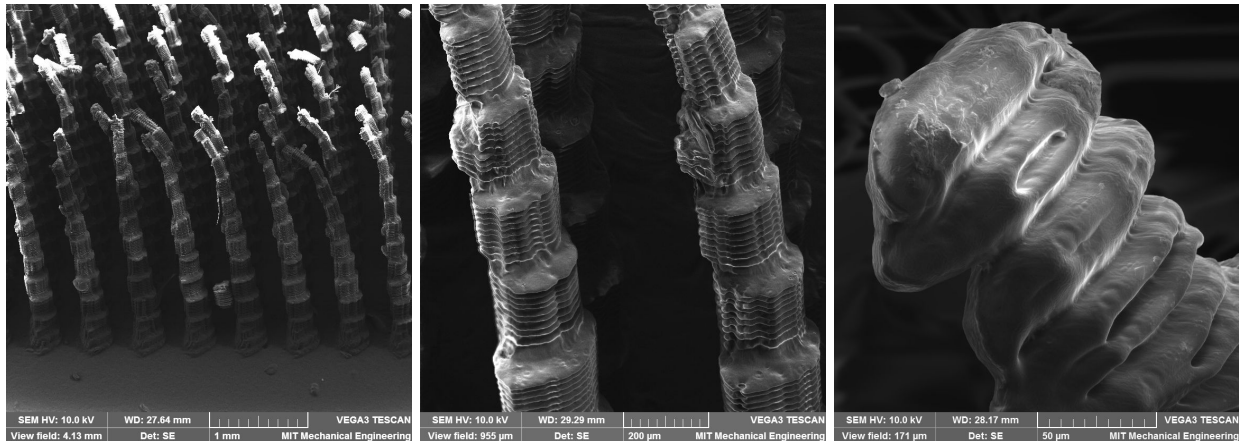


Figure 5. SEM images of the 3D-printed micro-pillars

B. Laser Micromachining and Replica Molding

One method we used to produce the micro-pillared surfaces involved laser micro-machining a mold which was then used to cast the PDMS surface. We used a 248nm Excimer laser (Resonetics RapidX250) with a 5-axis stage to drill blind holes in an acrylic sheet at various angles. The toolpath is generated using a custom script which maps an XY grid of desired angles (U and V) to the respective axes. This involves calculating coordinate offsets due to the off-axis center of rotation. The diameter of the hole can be varied by changing either the demagnification of the laser or by using a mask with a different size aperture. In this case, we used a 5mm mask with a demagnification factor of about 11x, resulting in a hole which is 450 μm at its widest point and tapers to a tip diameter of approximately 100 μm . The depth of the hole can be controlled with the number of pulses per spot. In this case we used 150 pulses per spot to create 800 μm deep holes.

The resulting acrylic can then be lightly rinsed in isopropyl alcohol, to remove any recast material, and used for PDMS replica molding. Because the features are quite small but deep, it is important to let the PDMS degass for upwards of thirty minutes to ensure any air bubbles trapped in the tips have time to escape. It is also important to let it cure for at least thirty minutes at 80°C so that the tips are firmly attached to the bulk of the substrate.

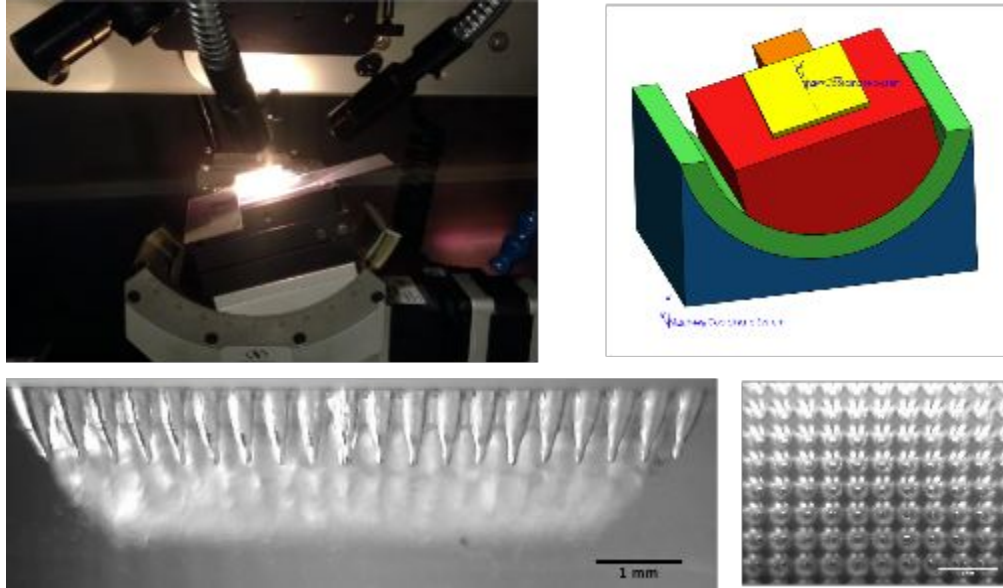


Figure 6. Excimer laser micro-machining acrylic molds.

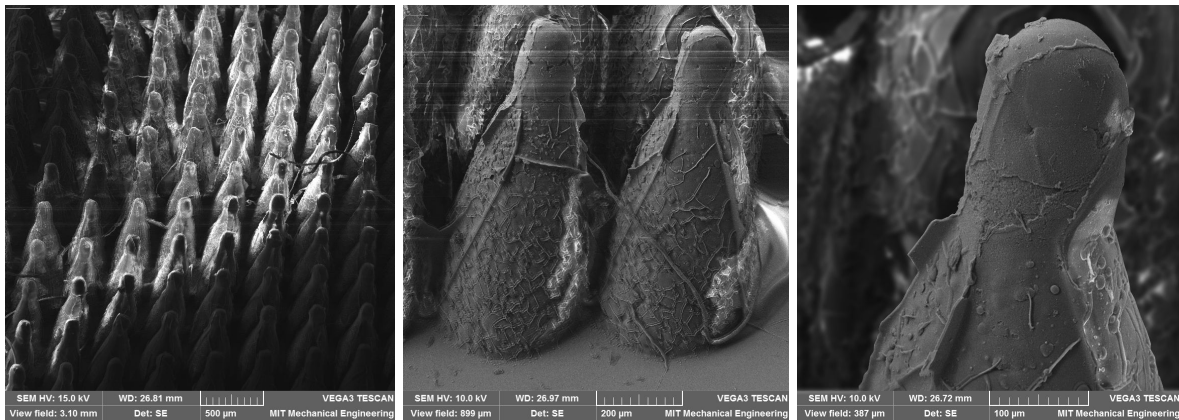


Figure 7. SEM images of the cast PDMS pillars.

VI. Experimental Setup

Our experimental setup consists of a piezo shaker table which vibrates the micro-pillared surface. The frequency and amplitude of this vibration can be precisely controlled with a function generator (Tektronix MDO3000 oscilloscope with built-in function analyzer) and high voltage piezo amplifier (Piezo Drive PDu100).

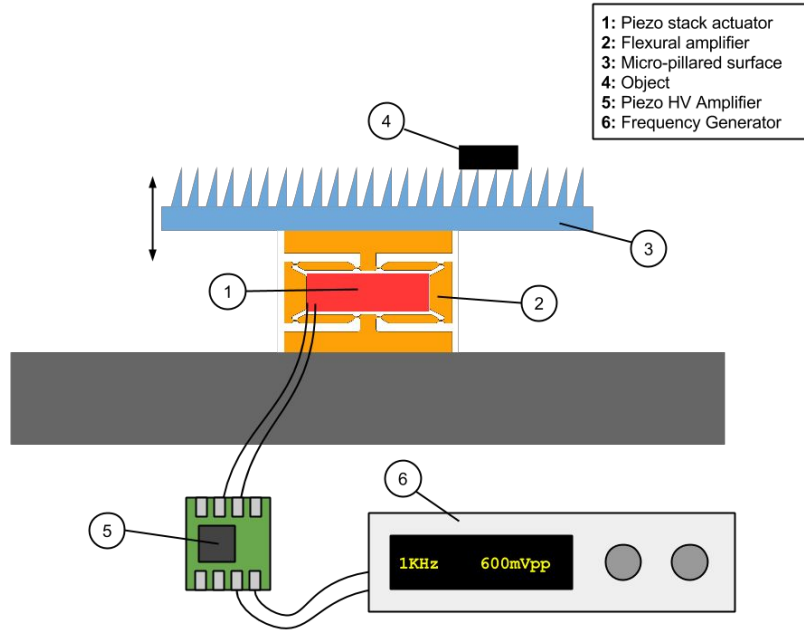


Figure 8. Diagram of experimental setup.

A. Piezo shaking mechanism

The piezo shaker mechanism comprises a 3mmx3mmx10mm 100V piezo stack actuator (ThorLabs PK3JMP2) embedded in a flexural amplifier. The flexural amplifier was cut from 3mm-thick 17-4 PH stainless steel using a wire-EDM. This mechanism is used to amplify the small ($\sim 9 \mu\text{m}$) displacement of the piezo stack by approximately 15 times to achieve a maximum amplitude of roughly $120 \mu\text{m}$.

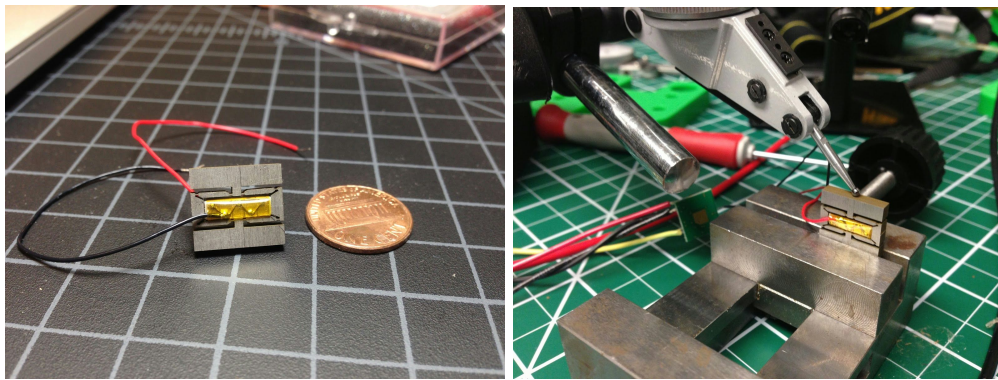


Figure 9. Piezo shaking mechanism.

For the experiments described in this work, the piezo is driven with a sawtooth waveform (a ramp with 100% symmetry). The surface, therefore, follows a trajectory involving a slow-rise and a quick fall. The amplitude of oscillation is tunable up to a maximum of $120 \mu\text{m}$ peak-to-peak and is controlled by the amplitude of the input voltage signal (for which 3.6Vpp corresponds to the maximum).

B. Sample Geometry

For the pillared surface, we fabricated two samples with stereolithography and replica molding. Both sample has identical pillar orientation. The array of pillars tilt in a way that the moving objects converge from two side to the center, while also moving forward (Figure 10).

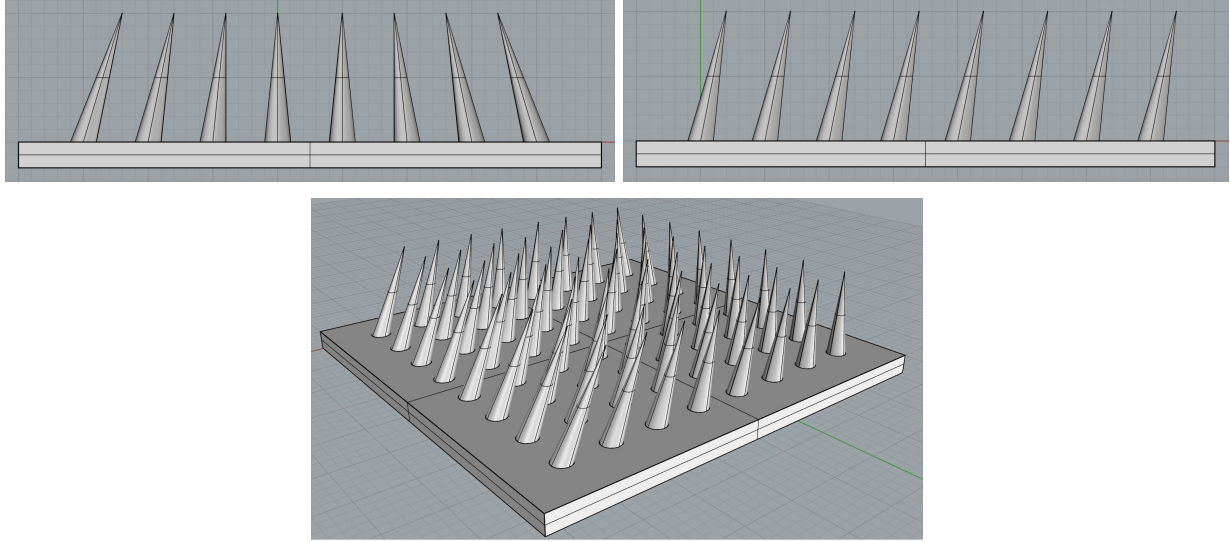


Figure 10. Simulation of the pillars' orientation. top left: front view. top right: left view. bottom: perspective view.

VII. Results

We first used a high-speed camera to qualitatively analyze the movement of the objects on the micro-pillared surfaces. Looking at the sequence of images pictured in Figure 10, it is clear that our initial hypotheses about the nature of the object's movement are not correct. For one, the motion is not perfectly planar (as it is assumed in the basic model); the part rocks backwards and forwards as it moves across the surface. Furthermore, it is clear that the deflection of the pillars is not the primary motive force. Instead, the object hops over the surface and moves more than the pitch of the pillars in a single pulse of the piezo.



Figure 11. Sequence of images taken from high-speed video of an object moving on the surface.

To get a further understanding of the parameters that contribute to the performance of this system, we ran a series of measurements to test the dependence the object's velocity on the frequency of oscillation, the amplitude of oscillation, and the mass of the object itself.

A. Velocity dependence on frequency of oscillation

To measure the dependence that the object's velocity has on the frequency of oscillation, we captured video and used image processing to calculate the average velocity over a series of frequencies ranging from 3Hz to 36Hz. The result, shown in Figure 12, clearly demonstrates that frequency and velocity are linearly related. This implies that the distance the object travels per pulse is independent of frequency and is approximately equal to the slope of the line (neglecting the zero-offset). On the PDMS substrate the object moved 695 μm per pulse and on the 3D-printed substrate the object moved 293 μm per pulse.

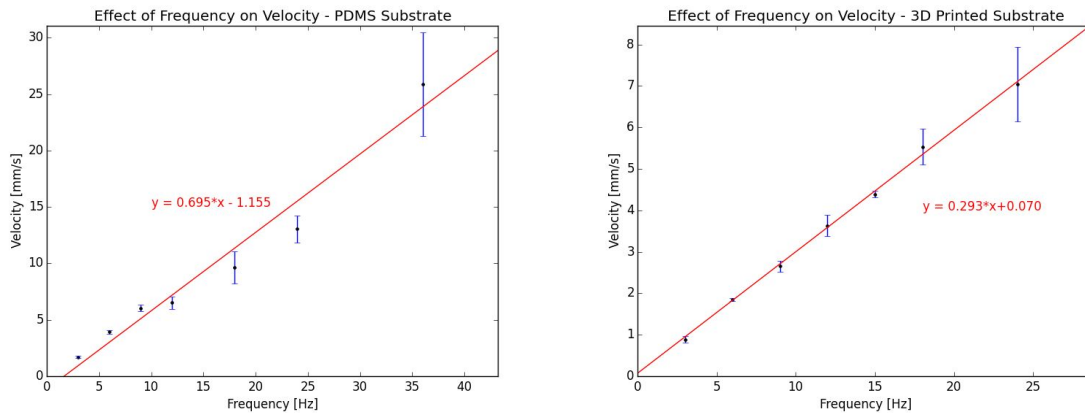


Figure 12. The effect of frequency on velocity of the object on the surface.

B. Velocity dependence on amplitude of oscillation

We used the same technique as above to measure the effect the amplitude of oscillation has on the object's velocity. We tested amplitudes ranging from 16 μm up to 116 μm . The result, shown in Figure 12, shows that amplitude and velocity are linearly related. This means that the mechanism that moves the object on the surface is likely a strong function of the magnitude of acceleration of the platform. As the amplitude is increased, the acceleration increases with it; this is particularly true for fast changing signals like our sawtooth waveform.

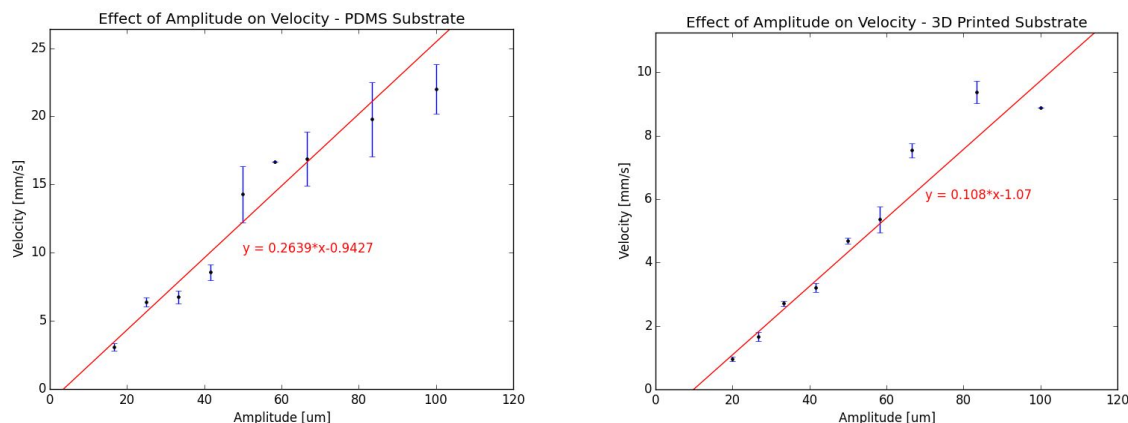


Figure 13. The effect of amplitude on velocity of the object on the surface.

C. Velocity dependence on object mass

Finally, we looked at the relationship between the object's mass and its velocity. To be able to vary the object's mass, we constructed it from lasercut stainless steel disks. This enabled us to sequentially stack the disks using adhesive to achieve a range of objects with varying mass but the same footprint. We found no strong dependence on mass based on our current test.

While results from 3D-printed sample (Figure 13-right) are not especially informative, the first four data points of the PDMS sample (Figure 13-left) are suggestive of a linear increase, which tentatively supports our initial prediction that the relationship between velocity and mass looks like a curve in which velocity increases relatively linearly with additional mass up to a certain point, and then decreases. This prediction was founded on the assumption that pillar deflection, rather than hopping, was the primary motive force of transport.

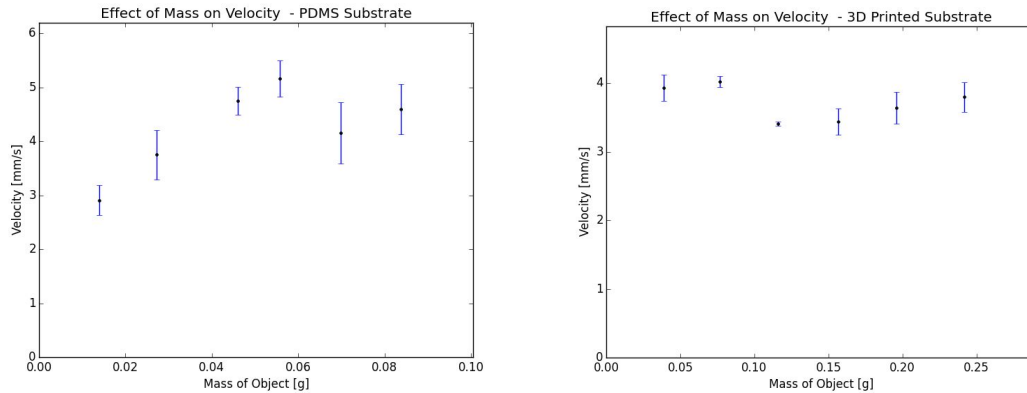


Figure 14. The effect of mass on velocity of the object on the surface.

There are a number of possible sources of error in this experiment. The first and foremost is that the fabrication process involved in making the test objects left non-smooth edges with burrs. Sanding with a fine grit sandpaper helped to remove most of the burr, but not all of it. Second, while the layer based process did not affect the footprint of the object, it did alter the height of the center of mass. The lightest object had a very different aspect ratio (thin, flat disk) than the heaviest object (which was much more cylindrical) and it is possible this influenced the results. Furthermore, the fabrication quality of the hair tips might affect how well the samples performs as well. The PDMS one performs more consistently compared to the 3D printed one, which might be due to the higher quality of its hair tips.

III. Potential Applications

The most basic capability of this kind of conveyance system is to move parts in a straight-line. We've shown that this can be accomplished with a surface of pillars that all point towards the center line (depicted in Figure 15). A part placed at one end of the center line travels in a straight-line to the other end of the line. This kind of surface also acts as a kind of funnel; a part placed in a corner of the surface first travels diagonally to the center line and then in a straight-line along the center line. That is to say, on a sufficiently long surface, a part may be placed in any initial position and leave in the same output position (along the center line).

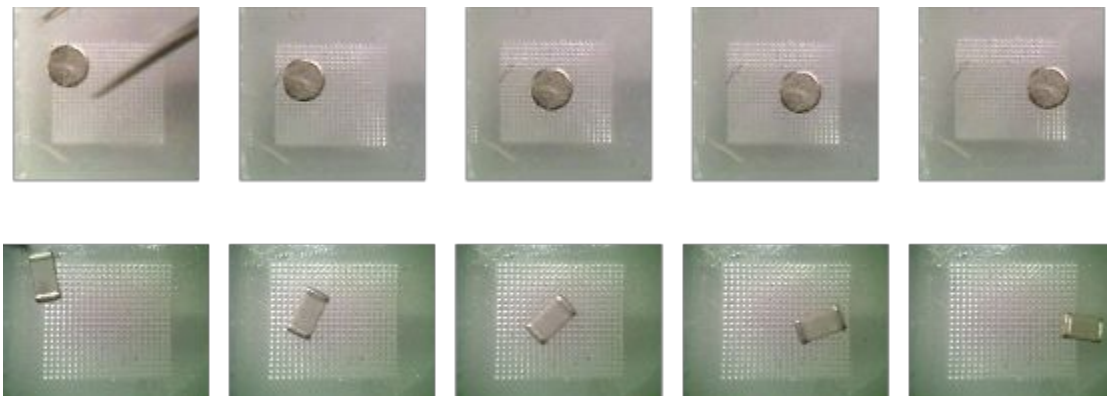


Figure 15. The same surface demonstrates both funneling (top) and

orienting (bottom) with different part-types.

For our future work, we would like to investigate the versatility of the system.

1. Orienting. This kind of surface may be used to orient parts. Parts that are not rotationally symmetric will experience asymmetric moments as they are transported, rotating the parts to the most stable orientation. This kind of orientation process is depicted in the figure below.
2. Sorting by size. Micro-pillared surfaces may be used to sort parts by size. The figure below depicts a sorting procedure in which parts are fed in from the left and parts smaller than a certain threshold are passed through to the right while larger parts are pushed to the top edge of the surface. We can also create path with different height to achieve this functionality.

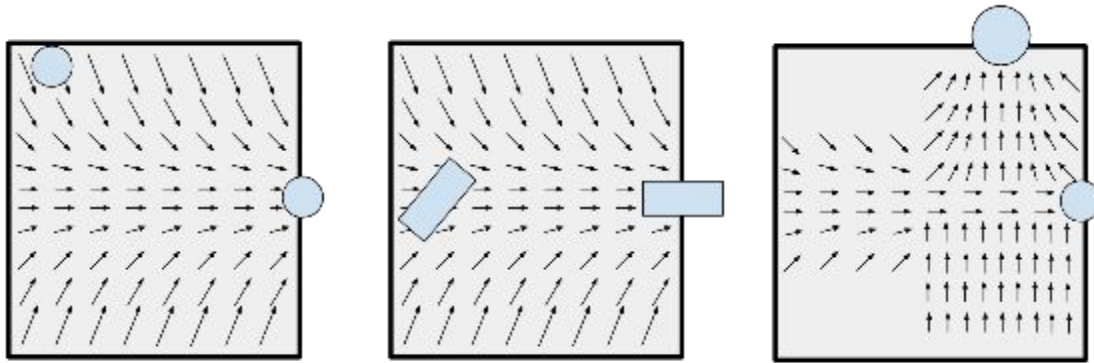


Figure 16. Three potential applications. Funneling parts (left). Orienting parts (middle). Sorting parts by size (right).

VIII. Conclusion

Inspired by natural cilia structures, our system explores the principle of anisotropic friction through structured surfaces of oriented micro-pillars that are subjected to a global vibration source. We have successfully built a system that has predictable parts transportation and orientation capabilities.

Several improvements are planned. Further mechanical tests with better fabricated micro-pillar arrays, a better choice of transported mass, and more data points will give us more conclusive empirical data on the experiments of velocity-mass dependence. A hybrid dynamic simulation may further improve the performance prediction. An automated workflow, starting from a graphical color map to a machining file containing instructions of pillar parameters, will increase the speed of manufacturing and provide bigger flexibility of design. Finally, we hope to build more applications, such as surface mounted electronic components sorting based on their size or mass, and animated moving objects for art and design.

References

- [1] A. Filippov and S. N. Gorb, "Frictional-anisotropy-based systems in biology: structural diversity and numerical model.," *Sci. Rep.*, vol. 3, p. 1240, Jan. 2013.
- [2] S. Gueron, K. Levit-Gurevich, N. Liron, and J. J. Blum, "Cilia internal mechanism and metachronal coordination as the result of hydrodynamical coupling," *Appl. Math.*, vol. 94, no. June, pp. 6001–6006, 1997.
- [3] M. Ataka, B. Legrand, L. Buchailot, D. Collard, and H. Fujita, "Design, Fabrication, and Operation of Two-Dimensional Conveyance System With Ciliary Actuator Arrays," *IEEE/ASME Trans. Mechatronics*, vol. 14, no. 1, pp. 119–125, Feb. 2009.
- [4] K.-F. Böhringer, B. R. Donald, and N. C. MacDonald, "Programmable Force Fields for Distributed Manipulation, with Applications to MEMS Actuator Arrays and Vibratory Parts Feeders," *Int. J. Rob. Res.*, vol. 18, no. 2, pp. 168–200, Feb. 1999.
- [5] T. Ebefors, J. U. Mattsson, E. Kalvesten, and G. Stemme, "A robust micro conveyer realized by arrayed polyimide joint actuators," *Tech. Dig. IEEE Int. MEMS 99 Conf. Twelfth IEEE Int. Conf. Micro Electro Mech. Syst. (Cat. No.99CH36291)*, pp. 576–581, 1999.
- [6] J. W. Suh, R. B. Darling, B. R. Donald, H. Baltes, and G. T. A. Kovacs, "CMOS Integrated Ciliary Actuator Array as a Tool for Small Objects," vol. 8, no. 4, pp. 483–496, 1999.
- [7] T. Tsao and P. Will, "A Micromachined Permalloy Magnetic Actuator Array for Micro Robotics Assembly Systems," *Proc. Int. Solid-State Sensors Actuators Conf. - TRANSDUCERS '95*, vol. 1, pp. 328–331, 1995.
- [8] G. Laurent, A. Delettre, R. Zeggari, R. Yahiaoui, J.-F. Manceau, and N. Fort-Piat, "Micropositioning and Fast Transport Using a Contactless Micro-Conveyor," *Micromachines*, vol. 5, no. 1, pp. 66–80, Feb. 2014.
- [9] R. S. Fearing, "A Planar Milli-Robot System on an Air Bearing," in *Robotics Research*, Springer London, 1996, pp. 570–581.
- [10] a DeSimone and a Tatone, "Crawling motility through the analysis of model locomotors: two case studies.," *Eur. Phys. J. E. Soft Matter*, vol. 35, no. 9, p. 85, Sep. 2012.
- [11] F. Becker, V. Lysenko, V. Minchenya, and I. Zeidis, "Romansy 19 – Robot Design, Dynamics and Control," vol. 544, no. 2005, 2013.
- [12] L. Giomi, N. Hawley-Weld, and L. Mahadevan, "Swarming, swirling and stasis in sequestered bristle-bots," no. Turner 2011, Feb. 2013.
- [13] A. Back, J. Guckenheimer, and M. Myers, "A Dynamical Simulation Facility for Hybrid Systems," *Lect. Notes Comput. Sci.*, vol. 736, pp. 255–267, 1993.